Organic-Inorganic Hybrid Thermocouple Intended for Thermoelectric Generators Using Low-Cost Nontoxic Materials

L. K. Narangammana[1] · Y. M. D. C. Y. Bandara[1] · L. Ajith DeSilva[2] · N. D. Subasinghe[3] · T. M. W. J. Bandara[1]

Abstract

Thermoelectricity, which converts heat energy directly into electricity, can be utilized as a waste heat recovery mechanism as well as an alternative energy resource. The thermoelectric generators (TEGs) consist of an array of *p–n* junctions made of two different thermoelectric materials (TEMs). TEGs can create a potential difference as a result of a temperature difference applied across the junction. Widely used and the best-known TEMs such as Bi_2Te_3 and Sb_2Te_3 are hazardous in nature. Therefore, there is an emerging need to search for new non-toxic TEMs. This study investigates the thermal, electrical, and thermoelectric properties of organic polyaniline (PANI) and the inorganic ceramic zinc oxide (ZnO). Further, it is extended to fabricate an organic/inorganic *p–n* junction suitable for hybrid TEGs using PANI and ZnO. Electrical conductivity and thermal conductivity of PANI, ZnO, and Al-doped ZnO (Al-ZnO) and the Seebeck coefficient, figures of merit and power factors of respective thermocouples were investigated. Fourier transform infrared spectroscopy and x-ray diffraction spectra confirmed the successful synthesis of PANI, ZnO, and Al-ZnO. The temperature-dependent electrical conductivity of all the compounds exhibits a semiconductor behavior. The temperature-dependent Seebeck coefficient of PANI and Al-ZnO are consistent with the values reported in the literature. However, ZnO showed a deviation. The PANI-ZnO thermocouple generated a potential difference of 21.16 mV at a temperature difference of 77 K and these materials indicate promising prospects of nontoxic and low-temperature TEMs.
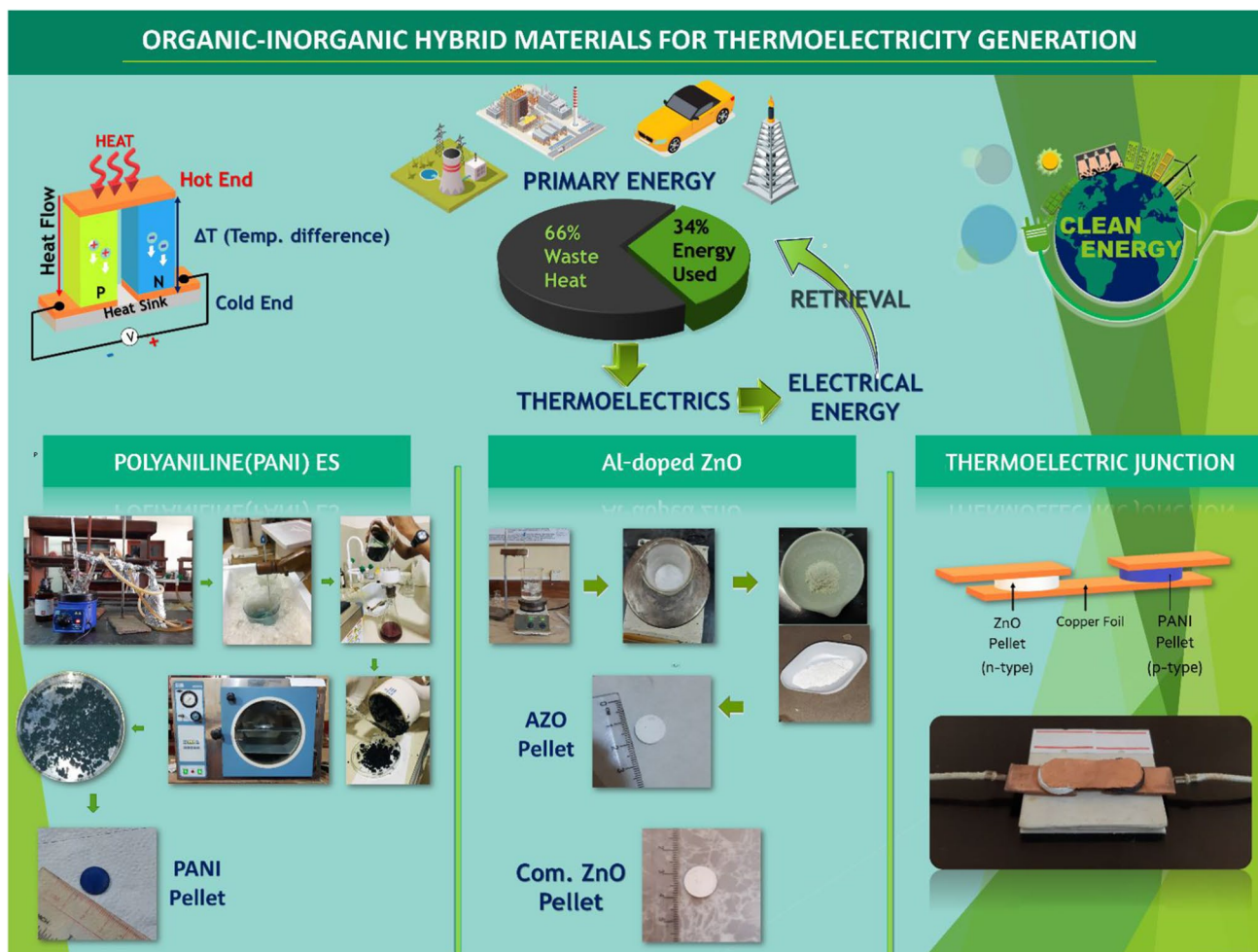
✉ T. M. W. J. Bandara
awijendr@yahoo.com

1 Department of Physics and Postgraduate Institute of Science, University of Peradeniya, Peradeniya, Sri Lanka

2 Department of Physics, University of West Georgia, Carrollton, GA 3011, USA

3 National Institute of Fundamental Studies, Hantana Road, Kandy, Sri Lanka

Graphical Abstract

Introduction

Global climate change and a shortage of fossil fuels have driven the need for alternative energy resources as well as for efficient energy conversion technologies.[1] In all the power generating systems, energy is lost, mainly as heat. Recovering some of the heat as a useful form of energy improves the efficiency of the system. Thermoelectricity is the direct conversion of thermal energy into electricity. This phenomenon is utilized in thermoelectric generators (TEGs) that have various applications such as recovering waste heat from industries, automobiles, and household activities. Thermoelectricity can also be utilized as an alternative energy conversion technology to harvest electricity from solar energy.[2,3] A TEG or thermoelectric junction device is a reliable and potentially scalable solid-state energy conversion system capable of generating electricity without greenhouse emissions. Further, TEGs are long lasting and silent in operation since they do not have any moving parts.

A TEG is made from an array of alternative arrangement of *p*-type and *n*-type semiconductors with different Seebeck coefficients, which are connected thermally in parallel and electrically in series. Once a temperature difference is applied across the TEG, or the stack of thermocouples, a resultant voltage is generated between the two sides. TEMs utilize the "Seebeck effect" for solid-state conversion of heat into electricity, where the Seebeck coefficient (α) is defined as the ratio between the generated voltage (ΔV) and the temperature difference (ΔT) across the thermocouple. The figure of merit (ZT) of a thermocouple is a measurement of its efficiency. The relationship between α, electrical conductivity

(σ), thermal conductivity (K) and ZT of a material is defined by the following equations.[4]

$$ZT = \frac{\sigma \alpha^2 T}{K} \tag{1}$$

$$\alpha = -\frac{\Delta V}{\Delta T} \tag{2}$$

The power factor (PF) is another parameter used to measure the efficiency of a TEM, given by

$$PF = \alpha^2 \sigma \tag{3}$$

A thermocouple consists of two types of materials. In one material (n-type), the electrons flow from the hot side to the cold side due to the difference in kinetic energy of the two sides. In the other material (p-type), the holes flow from the hot side to the cold side results in a potential difference between the two sides of the junction. When a material suitable for a thermocouple is heated from one end, the majority of the charge carriers will absorb this heat and eventually become energetic (Fig. 1). Thus, these carriers inherit higher kinetic energies and diffuse towards the colder side. As the charges accumulate at the cold end, the charge neutrality of the material is altered, creating a polarization leading to an electrical potential difference across the material. In the case of *n*-type semiconductors, in which the electrons act as the dominant carriers, the hot side becomes positively charged as the electrons diffuse away from it. In the case of *p*-type semiconductors, in which holes are dominant, the polarity is the opposite to that of *n*-type semiconductors.

When two types of materials (e.g. two different metals) are introduced to make a junction, electron diffusion can take place. This is due to the difference in electron concentrations in the two materials. This process of electron movement is enhanced under a temperature gradient due to thermally activated diffusion. Consequently, when two such junctions are
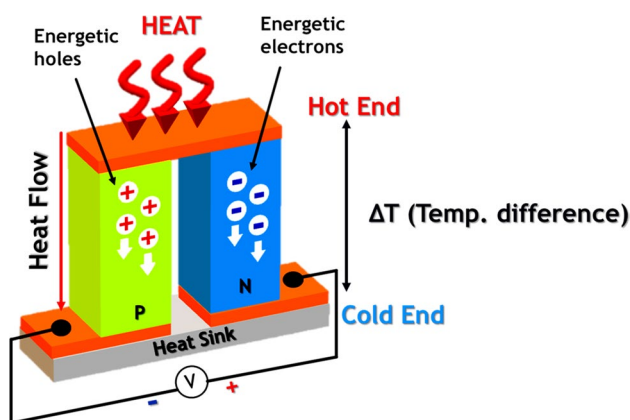

Fig. 1 Schematic illustration of thermoelectric power generation.

kept at two different temperatures, a significant potential difference can be gained at the two ends of the setup or (thermocouple). A better performing system can be realized when dealing with semiconductor materials in which an array of a *p–n* junctions form thermoelectric generators.

A high-performance thermoelectric material requires high σ, high α, and low K, and finding a material with that combination is challenging. In metals, σ is proportional to K where electron thermal conductivity is dominant. In semiconductors, σ is proportional to K where the lattice thermal conductivity is dominant. But the advantage of semiconductors is that σ and K can be easily tuned according to the desired condition through doping. For example, through doping, a high electrical conductivity can be achieved in a semiconductor maintaining a low thermal conductivity for the same doping concentration, which is the desirable condition for an efficient TEM. In this regard, semiconductors play an important role as thermoelectric materials due to their easily interchangeable electrical and thermal properties in order to fabricate efficient TEMs.

Extensive research has been carried out in search of novel TEMs as well as for improving the ZT of the existing TEMs with the intention of developing TEGs.[1-7] However, major drawbacks in most of the materials previously studied are the usage of rare earth or toxic elements, high fabrication cost, or poor mechanical properties. Because of the hazardous and rare earth nature of the best-known TEMs, such as bismuth telluride (Bi_2Te_3) and antimony telluride (Sb_2Te_3), there is a need to search for new nontoxic TEMs.[1] In addition, the fabrication cost and the poor mechanical properties of the existing TEMs are areas needing further improvement in this field. Investigation of conducting polymers and their composites for TEMs has become of interest due to their environmentally friendly nature and many other advantages such as low cost, easy fabrication processes, and a wide range of easily tunable electrical and thermal properties.[5,6] The polymers, in general, possess a low σ and low α compared to inorganic TEMs, which is a disadvantage for the overall performance of a TEM, but by adding appropriate dopants, this issue can be resolved. Because of the low K inherent to polymers, they became suitable candidates for TEMs. Recently, hybrid organic-inorganic TEMs have become an interesting candidate to fabricate TEGs. This is due to the low K contribution from the organic material and the high σ and α generated by the inorganic counterpart.

The *p*-type organic semiconductor/conductive polymer: polyaniline (PANI), has been widely used in thermoelectric power generation due to its promising thermoelectric properties.[7] Recently, Debnath et al.[8] reported a significant α value of 1767 μV K^{-1} of PANI/titanium oxide (TiO_2) nanocomposites which are potential candidates for novel TEGs. Incorporation of nickel oxide (NiO) into the PANI matrix also enhanced the value of α to 331 μV K^{-1} for a 0.75 %

doping of NiO by weight. For the same composition, the generated thermal electromotive force (emf) was 34 mV for a 104 K temperature difference indicating its usability as TEGs.[9] Very recently, Nayak et al.[10] fabricated a flexible TEG using screen printing of PANI and PANI/graphite based inks. The maximum reported Seebeck coefficient and power output were 24,4340 μV K^{-1} and 4.31 nW, respectively, at a temperature difference of 77 K. This novel flexible TEG constructed using screen printing opens up a new state-of-the-art for polyaniline based composite materials.

Thermoelectric properties of TEGs have been improved by using organic-inorganic composites rather than using a single material.[11] Li et al.[12] reported an organic–inorganic hybrid TEM suitable for TEGs using Bi_2Te_3/PEDOT:PSS and Te/PEDOT:PSS composites, which generated a voltage of 56 mV and power density of 32 μW cm^{-2} at a temperature difference of 60 K. In addition, Xu et al.[13] reported a maximum power density of 0.13 W m^{-2} at a temperature difference of 35.5 K for an organic-inorganic composite TEG based on polyvinylidene fluoride (PVDF). Further, thermoelectric properties of PANI films prepared by changing the m-cresol content in the solvent have led to improvements in σ from 4.7 S cm^{-1} to 220 S cm^{-1}, and the TEG exhibited the highest α of 20 μV K^{-1}.[14] Regarding thermoelectric properties of PANI/graphene composites, a σ of 856 S cm^{-1} and PF of 19 μW m^{-1} K^{-2} were reported.[15] Another study reported optimal σ, α and PF of 814 S cm^{-1}, 26 μV K^{-1}, 55 μW m^{-1} K^{-2} , respectively, for a TEG, which are the highest values among the reported polymer/graphene composite.[15] As reported by Liu et al.,[11] out of all the TEGs assembled using the PANI composites (prepared by molecular self-assembly) the highest α of 65 μV K^{-1} and PF of 176 μW m^{-1}K^{-2} were recorded for the material prepared with single-walled carbon nanotubes (SWCNT).[16] However, the performance of PANI-based TEM has been improved by doping which reported the highest α of 46.5 μV K^{-1} and PF of 401 μW m^{-1} K^{-2} for a PANI/SWCNT device.[17]

Zinc oxide (ZnO) is a potential candidate for high-temperature thermoelectric material (TEMs). ZnO is an n-type wide band gap semiconductor. Its band gap is between 3.2 eV and 3.5 eV and it has a high electron mobility and thermal conductivity.[18] Aluminum (Al)-doped ZnO (Al-ZnO), on the other hand, has received increasing attention due to its utilization in stable high-temperature thermoelectric power generation systems.[19] ZnO can be used to prepare bulk and thin-film TEG along with various structural morphologies with different dopant concentrations.[1,20] At room temperature, ZnO exhibited a PF of ~800 μW m^{-1} K^{-2} and thermal conductivity 40 W m^{-1} K^{-1}. Thermal conductivity decreases with increasing temperature, reaching 5 W m^{-1} K^{-1} at 100°C and the thermal conductivity varies from 40 W m^{-1} K^{-1} to 5 W m^{-1} K^{-1}. However, properties depend highly on the preparation method, structure, dopant

type, and concentrations. According to this study, α varies between -40 μV K^{-1} and -140 μV K^{-1} in a 350 K to 750 K temperature window.

Recently, a thin film TEG has been fabricated using ZnO as the n-type material and SnO$_x$ as the p-type material and the generated maximum output power for a 160 K temperature difference using four pairs of thermocouples was 126 μW cm^{-2}.[21] Klochko et al.[22] reported the construction of a flexible thin film TEG using ZnO and indium-doped ZnO thin films which produced a 0.8 μW m^{-2} at a temperature difference of 50 K. These reports stipulate the possibility of utilizing ZnO as a TEM to fabricate TEGs. In addition, using multiple dopants, sulfur (S), carbon(C), iron oxide (Fe_2O_3) and nickel oxide (NiO) simultaneously, the ZT value of bulk ZnO is significantly improved, showing the possibility of tuning the thermoelectric parameters of ZnO through doping.[23] Even though the thin film TEGs have been widely investigated, studies on bulk TEGs are still lacking. In this work, an effort has been made to investigate the thermoelectric properties of PANI-ZnO organic-inorganic p–n junctions to fabricate a thermocouple appropriate for low-temperature applications.

Experimental Details

Material Synthesis and Characterization

PANI emeraldine salt (PANI ES) was synthesized by chemical polymerization of aniline using sodium persulfate as the oxidant and 2 M HCl as the dopant. The prepared PANI ES product was dried at 55°C inside a vacuum oven for 24 h. Subsequently, Al-ZnO powder was synthesized by chemical co-deposition using $Zn(CH_3COO)_2 \cdot 2H_2O$ and $Al(NO_3)_2 \cdot 9H_2O$ in relevant proportions to achieve 1% of Al doping. Next, the Al-ZnO powder was annealed at 800°C for about 30 min. A low-pressure pellet synthesizing method was performed to produce samples. Each pellet with a diameter of 13 mm was fabricated using prepared PANI ES, Al-ZnO, and commercially available ZnO powder (AR, Fisher® Chemicals and Reagents) by applying a pressure of 295 MPa on wet samples. After pressing, both commercially available ZnO and synthesized Al-ZnO pellets were annealed at 800°C in a muffle furnace for 30 min, while the PANI pellets were annealed at 180°C for 1 h in an oven. Figure 2 shows images of the pellet samples prepared in this study.

The successful synthesis of PANI ES was confirmed by Fourier transform infrared (FTIR) spectroscopy in the wavenumber range of 400–4000 cm^{-1} with a resolution 1 cm^{-1} using a JASCO FT/IR 6700 instrument. Powder x-ray diffraction was performed for the crystallographic analysis of the synthesized Al-ZnO using a Rigaku Ultima

IV x-ray Diffractometer (XRD) (KYOWAGLAS-XATM, Japan) with Cu Kα radiation of $\lambda = 1.54184$ A°.

Single-Junction Device

P-type PANI ES and *n*-type ZnO pellets were arranged as in Fig. 3, to construct the thermoelectric single-junction device. As shown in Fig. 2, the lowermost surfaces of both pellets were fixed onto copper plates using silver adhesive, and subsequently, the top-most surfaces were linked to each other (*p–n*) using copper foil with silver adhesive such that two pellets were positioned electrically in series and thermally in parallel. The two connectors at each end were connected to a Keithley® source meter to measure the potential difference across the junction.

Thermoelectric Parameter Measurements

The electrical conductivities of pressed pellets of PANI ES, ZnO, and Al-ZnO were obtained using the resistance calculated from current versus voltage curves obtained via a PV Power Analyzer (SPD Labs, Japan). For this purpose, the current was measured by varying the applied potential from 0.5 V to 1.5 V. The thermal conductivity of the pellet samples was measured using absolute steady-state axial flow. The generated potential differences across the material and the corresponding applied temperature difference across the pellets were measured for all three material samples to calculate α. Here, each pellet was sandwiched between two electrodes, as shown in Fig. 3. The top-most electrode was in contact with a heatsink (cold end), while the other end was in contact with a heating strip (hot end). Here, an electrically non-conductive thermal paste was used at the interfaces to
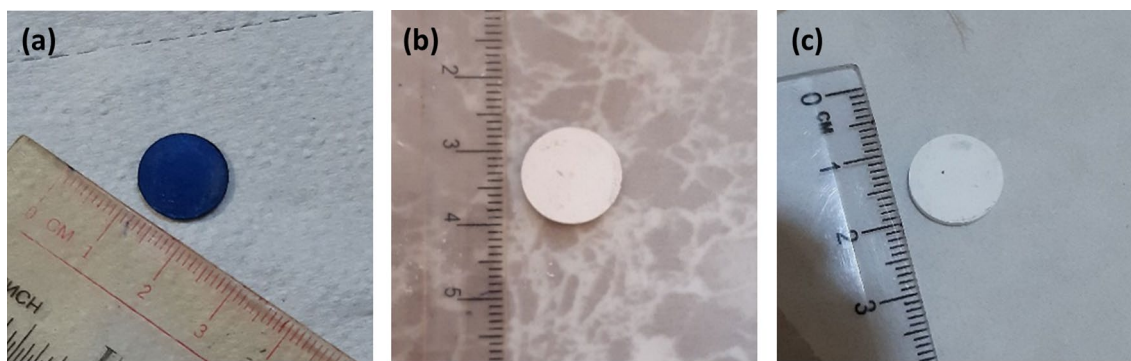

Fig. 2 Images of pellets prepared with (a) PANI, (b) Commercial ZnO, (c) Al-ZnO.
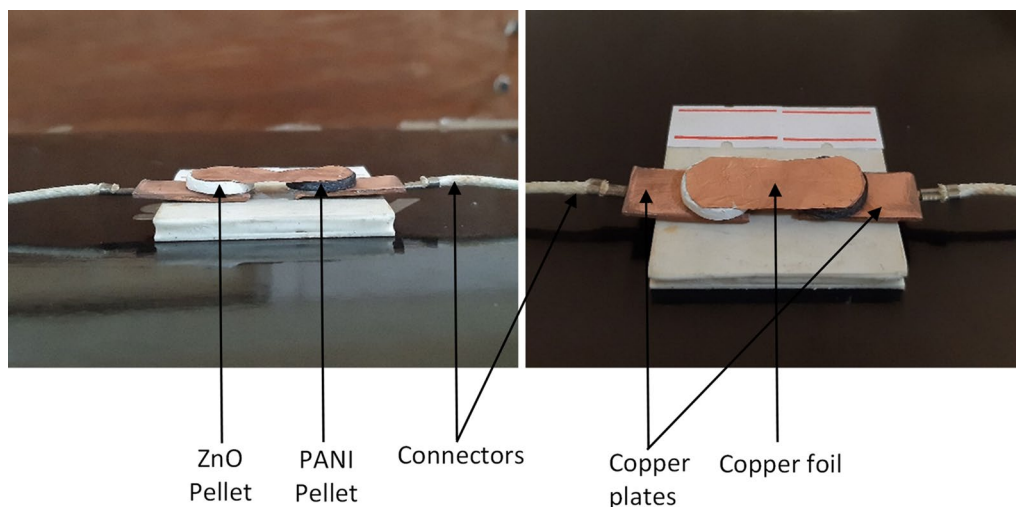

Fig. 3 Image of the PANI-ZnO thermoelectric single-junction device.

enhance the thermal flow. The silver adhesive was used to improve the electrical contacts between the pellets and the electrodes. An Extech® Easyview 15 dual-port thermometer with data logger software recorded temperatures at the hot and cold ends while a MATLAB program interfaced with the source meter recorded the potential differences at different temperature gaps simultaneously. A similar method was used for the thermoelectric junction of PANI and ZnO (single-junction device), where the top end of the junction was in contact with the heat sink while the other end was in contact with the heat strip. The temperature-dependent ZT and PF were calculated for PANI ES, ZnO, and Al-ZnO using their temperature-dependent α, σ and K using Eqs. 1 and 3.

The maximum power output of the single-junction thermoelectric device is calculated by measuring the output current and voltage by a Keithley 485 Autoranging Picoammeter and Keithley 2400 Series Source Meter, respectively, varying the load resistance. The contact area at the junction is 1.327 cm^2, which is equal to the cross-sectional areas of the pellets. The current density (j) is calculated by dividing current by the contact area at the junction.

Results and Discussion

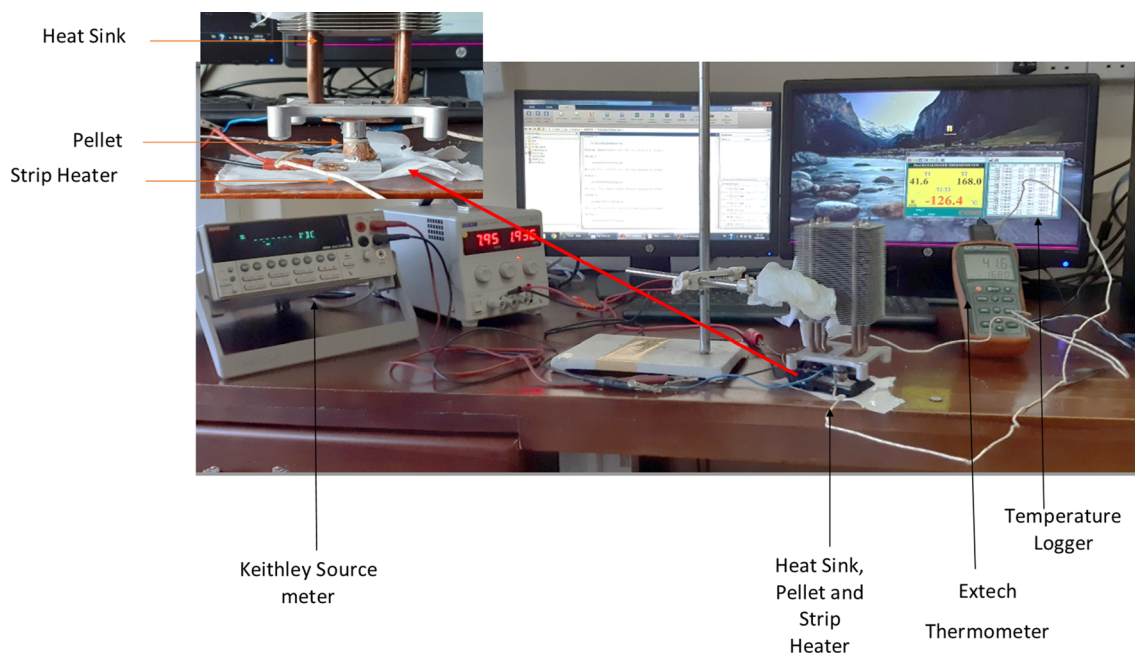Figure 5 shows the FTIR spectrum of PANI ES powder obtained using the attenuated total internal reflection (ATIR)

Fig. 4 Experimental setup to obtain the potential differences at different temperature gaps.
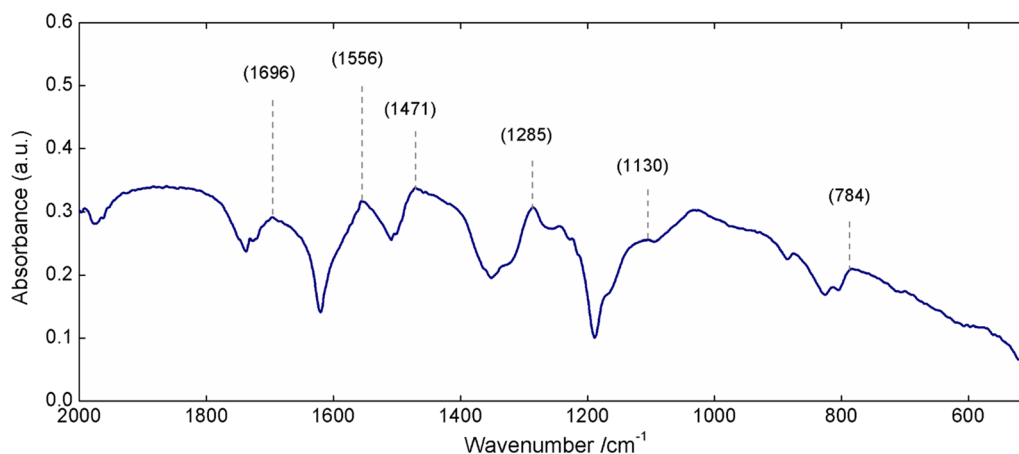

Fig. 5 FTIR spectrum of PANI ES prepared in this study.

mode. The peaks at wavenumbers 1556 cm^{-1} and 1471 cm^{-1} correspond to the stretching vibrations of C=N of quinone (Q) rings and stretching vibrations of C=C of benzene (B) rings, respectively. The peak at wavenumber 1285 cm^{-1} evidences the stretching vibrations of C–N secondary aromatic amines in the HCl-doped form of conducting PANI ES. A vibration mode of B-NH^{+}=Q structure, which is formed during protonation, is represented by the peak at wavenumber 1130 cm^{-1}. This is also a characteristic of conducting PANI ES.[24,25] Hence, the FTIR spectrum shown in Fig. 4 confirms the successful synthesis of conducting PANI ES (Fig. 5).

The powder XRD spectrum of ZnO and Al-ZnO is shown in Fig. 6. The crystal structure of the synthesized Al-ZnO matched well with the hexagonal wurtzite crystal structure of ZnO. There is no significant difference between the XRD patterns of ZnO and Al-ZnO. Also, no additional diffraction peaks were observed in the spectrum of Al-ZnO apart from the peaks related to the crystal planes of the original structure of ZnO (zincite). However, a slight broadening of the peaks can be observed. This small broadening could be due to the small crystallite size of Al-ZnO and may be the result of the substituted Al atoms in the lattice of ZnO, leading to the conclusion that Al has been substituted into certain Zn^{2+} sites of ZnO without forming any other phase. This evidences the successful synthesis of Al-doped ZnO. Unlike in some other studies, the peaks related to the phase of ZnAl$_2$O$_4$ could not be observed in this study.[9,12,13] This result highlights the successful Al doping without forming any other phases or compounds and can be attributed to the appropriate dopant concentrations used in the present study.

Figure 7a shows the temperature-dependent σ of PANI ES, ZnO, and Al-doped ZnO pellets. The σ of all three materials increased as temperature increased, verifying the
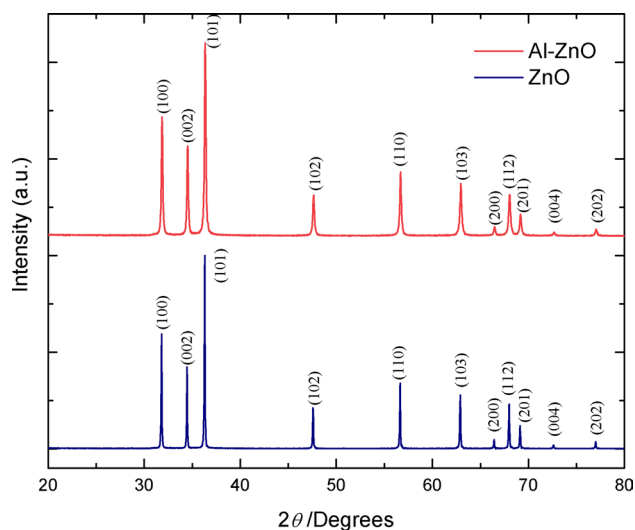

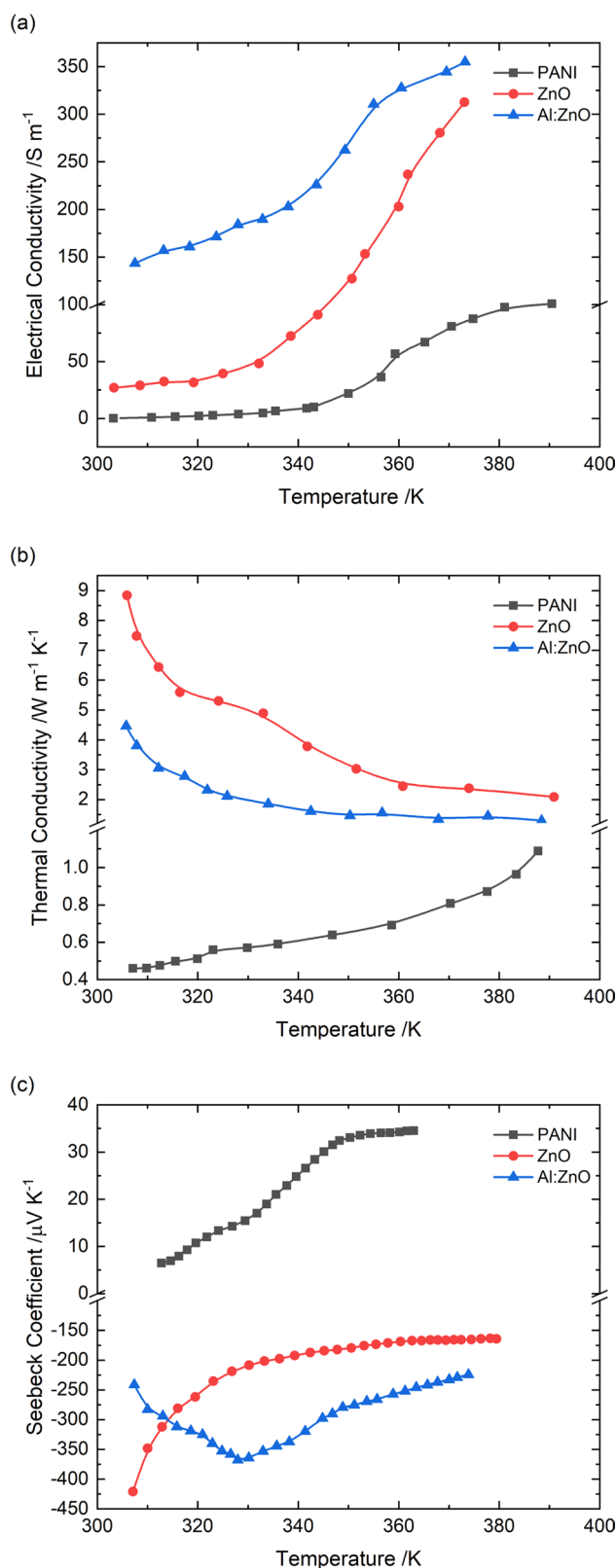**Fig. 6** Powder x-ray diffraction spectrum of ZnO and Al-ZnO.

Fig. 7 The temperature-dependent (a) electrical conductivity, (b) thermal conductivity, and (c) coefficient of PANI ES, ZnO, and Al-ZnO.

behavior of a semiconductor. The backbone of PANI consists of a chain of alternating single and double bonds in quinoid and benzenoid rings. Their overlapping *p*-orbitals create a system of delocalized π electrons, which contributes to σ. Unlike in intrinsic semiconductors, where electrons and holes are charge carriers, the charge transport in PANI occurs through polarons and bipolarons.[28,29] The rapid increase in σ above 340 K of PANI ES can be attributed to the thermally activated delocalization of polarons which are the majority carriers in conducting PANI ES.[14,15] The values and the temperature dependent behavior of σ of PANI is consistent with the results shown by Abed et al.[31] According to Wang et al., the highest electrical conductivity of PANI can be obtained by protonating all the imine sites with an acid.[32] Hence, to optimize the σ of PANI, a systematic study should be carried out by varying the doping concentration of the acid and hence the amount of protonation. The change of the doping agent to *p*-toluenesulfonic acid or camphorsulfonic acid is another method to optimize the σ of PANI. The ZnO sample with Al doping (Al-ZnO) has significantly high σ compared to pure ZnO at all temperatures, and the results are in agreement with the literature.[26] A higher σ of 35.6 S m^{-1} at 373 K in Al-ZnO can be attributed to the increased charge carrier density with the added Al donors. In this study, unlike in some other studies observed, an evolution from semiconductor to metallic behavior in σ of ZnO is not observed along with Al doping within the concentrations used, confirming the successful doping.[19,27] However, more studies are required to carefully optimize the Al concentration to improve the electrical conductivity of Al-ZnO without changing the material.

Figure 7b exhibits the temperature-dependent K of PANI ES, ZnO, and Al-ZnO. As the temperature increases, K of PANI increases and the results are consistent with other studies.[33] As the temperature increases, K of ZnO and Al-ZnO decreases, which is also consistent with the previous studies.[26,27,34] It is evident that the Al doping decreased the K of Al-ZnO compared to that of ZnO where the K of ZnO and Al-ZnO are 5.26, 2.17 W m^{-1} K^{-1} at 325 K, and they increase and decrease to 2.38 W m^{-1} K^{-1} and 1.40 W m^{-1} K^{-1}, respectively, at 373 K. This may be attributed to the random disordered phonon scattering induced

by the Al-deficient sites. The observed lower K in Al-ZnO is important since the lower K is an essential property of TEMs used in the TEGs to effectively maintain a higher temperature difference between the two ends. According to these results, with a larger amount of Al doping concentration, lower K values can be expected to enhance the overall performance of the TEM.

Figure 7c shows the temperature-dependent α of PANI ES, ZnO, and Al-ZnO. PANI ES exhibits a positive α while ZnO and Al-ZnO depict negative α, confirming the *p*-type semiconductor behavior of PANI ES and *n*-type semiconductor behavior of ZnO and Al-ZnO. Because of the low mobility rate of the polarons through the polymer chain compared to electrons, PANI ES exhibits low α values compared to that of ZnO and Al-ZnO. An increase in the absolute α with an increase in temperature can be observed for PANI, which is consistent with previous studies,[35] but ZnO shows a decrease in absolute α with the increase of temperature showing anomalous behavior. Al-ZnO shows an increase in absolute α up to 330 K to a value of $-375\ \mu$V K^{-1}, then a decrease to a value of $-250\ \mu$V K^{-1} at a higher temperature of 373 K, as observed in other studies.[26,27] This increase is related to the scattering of the lattice with atoms at an elevated temperature, and the decrease may be attributed to the rapid increase of intrinsic carrier concentration with a further increase in temperature.

The calculated *ZT* and *PF* for PANI ES, ZnO, and Al-ZnO at some temperatures are shown in Table I. The temperature-dependent evolution of the *ZT* of PANI ES, ZnO, and Al-ZnO are depicted in Fig. 8a. The ZT value of PANI ES increases with the temperature up to a maximum value of 37.4×10^{-7} at 363 K. The temperature-dependent behavior of ZT of PANI is consistent with another report,[35] but the magnitude of temperature-dependent ZT values are two orders lower, compared to this study. The temperature evolution of ZT values of both ZnO and Al-ZnO also showed an increase with maximum values of 1336×10^{-7} and 4801×10^{-7}, respectively, at 373 K, consistent with other reports, but the magnitude of temperature-dependent ZT values were hard to compare due to the inconsistent values reported in the literature.[19,26,27,36] The temperature dependent behavior of PF values of PANI ES, ZnO and Al-ZnO

Table I σ, *K*, α and ZT of PANI, ZnO, Al doped ZnO pellets prepared in this study at different temperatures

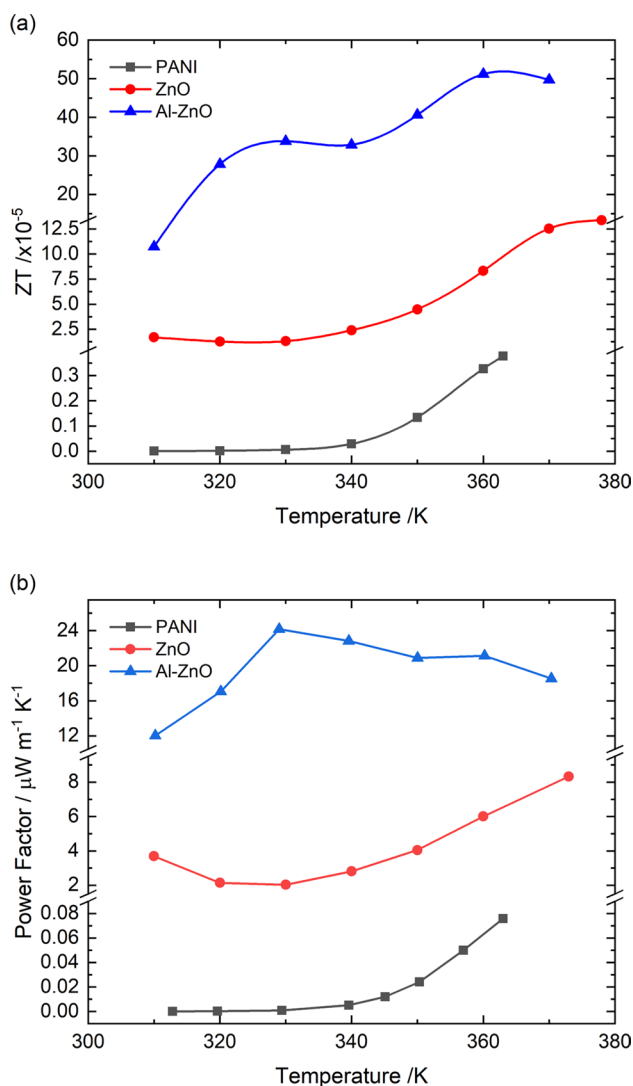| Material	$T = 325$ K			$T = 343$ K			$T = 363$ K	$T = 373$ K	
	PANI	ZnO	Al doped ZnO	PANI	ZnO	Al doped ZnO	PANI	ZnO	Al doped ZnO
σ ($\times 10^{-1}$ S m^{-1})	3.13	39.2	176	10.4	89.3	225	63.6	313	356
K ($\times 10^{-1}$ W m^{-1} K^{-1})	5.59	52.6	21.7	6.22	37.3	16.06	7.38	23.8	14.0
α (μV K^{-1})	14.1	-230	-353	28.4	-187	-300	34.6	-165	-225
(ZT) ($\times 10^{-7}$)	0.36	128	3280	4.61	287	3.61	37.4	1336	4801
PF (μW m^{-1} K^{-1})	0.0006	2.1	20.8	0.01	3.2	22.2	0.08	8.3	18.6

(a)

(b)

Fig. 8 The temperature-dependent (a) figure of merit (*ZT*), and (b) power factor of PANI ES, ZnO, and Al-ZnO.

Fig. 9 The generated potential difference as a function of applied temperature difference for the PANI-ZnO single junction device.

are shown in Fig. 8b. The PF values of PANI ES and ZnO remain almost constant from 310 K to 340 K but increase at higher temperatures. However, the PF value of Al-ZnO increases up to 24.1 μW m^{-1} K^{-1} at 330 K and decreases at higher temperatures. After doping, the PF value of Al-ZnO was increased by an order of magnitude compared to that of ZnO which is consistent with other reports.[19,26] The temperature evolution of PF of ZnO and Al-ZnO are consistent with these reports, but the magnitude of PF values in this study are two orders low compared to the values reported in these reports.

The generated potential difference resulting from the applied temperature difference between the hot and cold ends of the thermocouple is shown in Fig. 9. A maximum 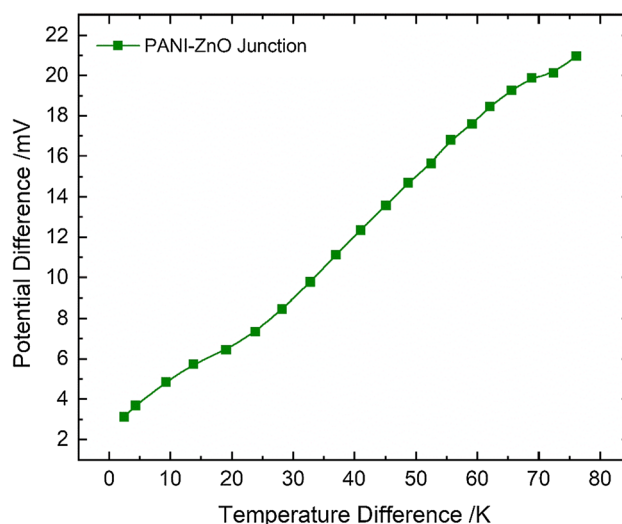of 21.16 mV within the measurement temperature window was achieved at a difference of 77 K temperature. Debnath et al.[8] reported a thermal emf value of approximately 12.5 mV for a temperature difference of 75 K for the optimized composition of PANI/TiO$_2$ composite. The reported thermoelectric voltage values of ZnO and indium-doped ZnO thin films by Klochko et al.[22] at a temperature difference of 40 K are 3 mV and 6 mV, respectively. For the optimized composition of PANI/NiO composite, the generated thermal emf value for a 104 K temperature difference was 34 mV.[9] These reports indicate the remarkable performance shown by the fabricated PANI/ZnO thermocouple in this study. The further improvement of PANI/ZnO thermocouple as a junction device holds promise as an effective TEG for low-temperature applications (Fig. 9).

It was observed that the single junction device gives 0.71 μA and 29 mV at a 101 K temperature difference. Hence, the current density and the maximum power densities of the device are 0.54 μA cm^{-2} and 15.51 nW cm^{-2} respectively.

Up to date, extensive research has been done to improve the thermoelectric properties of PANI. Several effective processing methods such as doping engineering, modulation of molecular orientation, inorganic nanoparticles incorporation and interface engineering have been applied to enhance the thermoelectric efficiency of PANI.[11] PANI thin films have been used as a conductive coating to enhance the thermoelectric efficiency of inorganic thin film TEGs.[37] PANI/graphite composites were used to fabricate thin-film TEGs using screen printing.[10] However, the utilization of PANI as a bulk TEG is very rare. ZnO as a thin film TEG has been studied in depth[21,22,38] but the studies of ZnO as a bulk TEG are rare. In this study,

we fabricated a bulk thermocouple selecting PANI as a *p*-type material and ZnO as an *n*-type material which holds promise as an effective thermoelectric generator. Further improvements should be made by enhancing the thermoelectric efficiency of the PANI and ZnO through doping and improving the device fabrication by using several legs, improving the connections between legs, etc.

Conclusion

Thermocouples based on PANI ES and ZnO pellets were successfully prepared, and the temperature evolution of σ, K, and α of PANI ES, ZnO and Al-ZnO were analyzed. σ values of ZnO and Al-ZnO pellets prepared in this work are 3.92 S m^{-1} and 17.6 S m^{-1}, respectively, at 325 K, and they increase to 2.38 S m^{-1}, 35.6 S m^{-1} at 373 K, respectively. K values of ZnO and Al-ZnO are 5.26 W m^{-1} K^{-1}, 2.17 W m^{-1} K^{-1} at 325 K, and they increase and decrease to 2.38 W m^{-1} K^{-1} and 1.40 W m^{-1} K^{-1}, respectively, at 373 K. σ, K, α and ZT of PANI ES pellets are 0.31 S m^{-1}, 0.56 W m^{-1} K^{-1}, 14.1 μV K^{-1}, 0.36×10^{-7}, respectively, at 325 K and they all increases except K with increasing temperature.

The thermocouple made from *p*-type PANI ES and *n*-type ZnO showed a maximum potential difference of 21.16 mV for a temperature difference of 77 K. From the combined literature, it is clear that the bulk studies on TEGs combining PANI and ZnO have been not done so far. There are fewer reported potential difference values for thin-film TEGs which consist of PANI and ZnO composites compared to the potential difference value we reported in this study. Therefore, the present study reveals that *p*-type PANI ES and *n*-type ZnO are suitable thermocouple materials for the preparation of low-temperature bulk thermoelectric generators. The dopant acid improves the thermoelectric properties of PANI ES. In addition, appropriate Al doping increases the σ of ZnO while it decreases K, and thus Al-ZnO is a promising material to prepare TEGs. Fabricated Al-ZnO pellets recorded α and ZT value of -353 μV K^{-1} 3280×10^{-7}, respectively. The maximum power density of the single junction device is 15.51 nW cm^{-2}. The thermoelectric properties of these devices can be further enhanced by optimizing the various parameters involved.

Conflict of interest On behalf of all authors, the corresponding author states that there is no conflict of interest.

References

1. O. Caballero-Calero, J.R. Ares, and M. Martín-González, *Adv. Sustain. Syst.* 5, 2100095 (2021).
2. I. Petsagkourakis, K. Tybrandt, X. Crispin, I. Ohkubo, N. Satoh, and T. Mori, *Sci. Technol. Adv. Mater.* 19, 836 (2018).
3. D. Champier, *Energy Convers. Manag.* 140, 167 (2017).
4. N. Jaziri, A. Boughamoura, J. Müller, B. Mezghani, F. Tounsi, and M. Ismail, *Energy Rep.* 6, 264 (2020).
5. M. Culebras, C. Gómez, and A. Cantarero, *Materials (Basel)* 7, 6701 (2014).
6. N. Dubey and M. Leclerc, *J. Polym. Sci. Part B Polym. Phys.* 49, 467 (2011).
7. Z.A. Boeva and V.G. Sergeyev, *Polym. Sci. Ser. C* 56, 144 (2014).
8. A. Debnath, K. Deb, K. Sarkar, and B. Saha, *J. Electron. Mater.* 49, 5028 (2020).
9. K. Sarkar, A. Debnath, K. Deb, A. Bera, and B. Saha, *Energy* 177, 203 (2019).
10. R. Nayak, P. Shetty, M. Selvakumar, A. Rao, and K.M. Rao, *Energy* 238, 121680 (2022).
11. S. Liu, H. Li, P. Li, Y. Liu, and C. He, *CCS Chem.* 3, 2547 (2021).
12. C. Li, F. Jiang, C. Liu, W. Wang, X. Li, T. Wang, and J. Xu, *Chem. Eng. J.* 320, 201 (2017).
13. Q. Xu, S. Qu, C. Ming, P. Qiu, Q. Yao, C. Zhu, T.-R. Wei, J. He, X. Shi, and L. Chen, *Energy Environ. Sci.* 13, 511 (2020).
14. Q. Yao, Q. Wang, L. Wang, Y. Wang, J. Sun, H. Zeng, Z. Jin, X. Huang, and L. Chen, *J. Mater. Chem. A* 2, 2634 (2014).
15. L. Wang, Q. Yao, H. Bi, F. Huang, Q. Wang, and L. Chen, *J. Mater. Chem. A* 3, 7086 (2015).
16. Q. Yao, Q. Wang, L. Wang, and L. Chen, *Energy Environ. Sci.* 7, 3801 (2014).
17. H. Li, S. Liu, P. Li, D. Yuan, X. Zhou, J. Sun, X. Lu, and C. He, *Carbon N. Y.* 136, 292 (2018).
18. K.P. Ong, D.J. Singh, and P. Wu, *Phys. Rev. B Condens. Matter Mater. Phys.* 83, 115110 (2011).
19. T. Tsubota, M. Ohtaki, K. Eguchi, and H. Arai, *J. Mater. Chem.* 7, 85 (1997).
20. A. Serrano, O. Caballero-Calero, M.Á. García, S. Lazić, N. Carmona, G.R. Castro, M. Martín-González, and J.F. Fernández, *J. Eur. Ceram. Soc.* 40, 5535 (2020).
21. E.M.F. Vieira, J.P.B. Silva, K. Veltruská, C.M. Istrate, V. Lenzi, V. Trifiletti, B. Lorenzi, V. Matolín, C. Ghica, L. Marques, O. Fenwick, L.M. Goncalves, and A.C.S. Appl, *Mater. Interfaces* 13, 35187 (2021).
22. N.P. Klochko, K.S. Klepikova, I.V. Khrypunova, D.O. Zhadan, S.I. Petrushenko, V.R. Kopach, S.V. Dukarov, V.M. Sukhov, M.V. Kirichenko, and A.L. Khrypunova, *Curr. Appl. Phys.* 21, 121 (2021).
23. B. Zhu, C. Chen, Z. Yao, J. Chen, C. Jia, Z. Wang, R. Tian, L. Tao, F. Xue, and H. Hng, *J. Eur. Ceram. Soc.* 41, 4182 (2021).
24. M. Trchová, I. Šeděnková, E. Tobolková, and J. Stejskal, *Polym. Degrad. Stab.* 86, 179 (2004).
25. M. Trchová and J. Stejskal, *Pure Appl. Chem.* 83, 1803 (2011).
26. S. Jantrasee, P. Moontragoon, and S. Pinitsoontorn, *J. Semicond.* 37, 092002 (2016).
27. X. Qu, W. Wang, S. Lv, and D. Jia, *Solid State Commun.* 151, 332 (2011).
28. A. Macdiarmid, G. Alan, and J.C. Chiang, *Synth. Met.* 13, 193 (1986).
29. P.N. Adams, P.J. Laughlin, S. Road, and S. Road, *Polymer (Guildf)* 37, 3411 (1996).
30. S. Stafström, J.L. Brédas, A.J. Epstein, H.S. Woo, D.B. Tanner, W.S. Huang, and A.G. MacDiarmid, *Phys. Rev. Lett.* 59, 1464 (1987).

31. M.Y. Abed, M.A. Youssif, H.A. Aziz, and M.A. Shenashen, *Egypt. J. Pet.* 23, 271 (2014).

32. R.-X. Wang, L.-F. Huang, and X.-Y. Tian, *J. Phys. Chem. C* 116, 13120 (2012).

33. P.B. Kaul, K.A. Day, and A.R. Abramson, *J. Appl. Phys.* 101, 083507 (2007).

34. T. Olorunyolemi, A. Birnboim, Y. Carmel, O.C. Wilson, I.K. Lloyd, S. Smith, and R. Campbell, *J. Am. Ceram. Soc.* 85, 1249 (2002).

35. J. Li, X. Tang, H. Li, Y. Yan, and Q. Zhang, *Synth. Met.* 160, 1153 (2010).

36. K.F. Cai, E. Müller, C. Drašar, and A. Mrotzek, *Mater. Sci. Eng. B Solid-State Mater. Adv. Technol.* 104, 45 (2003)

37. M. Kim, D. Park, and J. Kim, *Polymers (Basel)* 13, 1518 (2021).

38. S. Dalola, G. Faglia, E. Comini, M. Ferroni, C. Soldano, D. Zappa, V. Ferrari, and G. Sberveglieri, *Procedia Eng.* 47, 346 (2012).